Since January 2020 Elsevier has created a COVID-19 resource centre with free information in English and Mandarin on the novel coronavirus COVID-19. The COVID-19 resource centre is hosted on Elsevier Connect, the company's public news and information website.

Sensors & Actuators: B. Chemical 276 (2018) 437–446

Contents lists available at ScienceDirect

Sensors and Actuators B: Chemical

journal homepage: www.elsevier.com/locate/snb

Microorganism-ionizing respirator with reduced breathing resistance suitable for removing airborne bacteria

Miri Park[a], Ahjeong Son[a,*], Beelee Chua[b,*]

[a] Department of Environmental Science and Engineering, Ewha Womans University, 52 Ewhayeodae-gil, Seodaemun-gu, Seoul, 03760, Republic of Korea
[b] School of Electrical Engineering, Korea University, 145 Anam-ro, Seongbuk-gu, Seoul, 02841, Republic of Korea

ARTICLE INFO

Keywords:
Airborne microorganisms
Bacteria
Ionizer
Respirator
Breathing resistance
Corona ionizer

ABSTRACT

In this paper, we have demonstrated the feasibility of using microorganism-ionizing respirators with reduced breathing resistance to remove airborne bacteria. Using a miniaturized corona ionizer and two pairs of separator electrodes, airborne bacteria were ionized and removed from the airflow. Two microorganism-ionizing respirator designs were experimentally evaluated with flow rates ranging from ~10 to 20 L/min and yielded airborne bacterial removal efficiencies of ~75%–100%. Further, they were in close agreement with the analytical airborne particle removal efficiencies, at a similar range of flow rates. These flow rates also correspond to the breathing rates of standing and walking adults. More importantly, the breathing resistance could be reduced by more than 50% for flow rates of ~200 L/min. Using manganese (IV) oxide coated mesh, the ozone concentration in the air outflow was reduced to less than 0.1 ppm, at a flow rate of ~20 L/min, thus enabling safe use. The power consumption was less than 1 W.

1. Introduction

Airborne pathogenic outbreaks are a recurring theme in apocalyptic movie scenarios, where a deadly bacterium or virus rapidly transmits from human to human through the air. Exactly 100 years ago, the 1918 flu pandemic took its toll with at least 50 million dead and 500 million infected [1]. Recent airborne pathogenic viral outbreaks such as severe acute respiratory syndrome in 2003 and middle east respiratory syndrome in 2015, managed to spread across tens of countries causing multiple deaths [2–5]. In addition to viruses, there arehighly contagious airborne bacteria that can be transmitted person-to-person, causing diseases such as whooping cough (*Bordetella pertussis*), diphtheria (*Corynebacterium diphtheriae*), and tuberculosis (*Mycobacterium tuberculosis*) [6–8]. In the 1990 s, there were over 20 million cases of whooping cough worldwide, resulting in over 200,000 deaths [9]. In 2009, worldwide deaths due to tuberculosis were estimated at ~150,000 [10]; in 2013 alone, there were almost half a million tuberculosis cases [11]. Airborne transmission between humans occurs via respiratory droplets, with sizes ranging from 0.58 to ~5 μm [12,13].

In the event of an outbreak, the health advisories and precautions issued by the Health Protection Agency of the United Kingdom (HPA UK) and the United States Centers for Disease Control and Prevention (US CDC) was often limited to the use of N95 or higher-grade respirators to minimize further exposure and transmission [12,14,15]. Existing N95-based respirators employ woven fibers for mechanical filtration via inertia impaction, interception and diffusion to remove airborne particles and microorganisms from the air stream [16,17].

Unfortunately, the use of mechanical filtration is also accompanied by an increase in breathing resistance. Breathing resistance could increase by more than 100%, with a ~40% reduction in air exchange volume [18]. Further, with the gradual loading of particles on the mechanical filter, the pressure drop could also increase, by as much as a factor of 10 [19]. Therefore, associated discomfort and impaired breathing are not uncommon [20]. When used long-term, these problems can result in either the wearer loosening the respirator, causing improper fitting, or a complete avoidance. Mechanical filtration can also be augmented electrostatically (electret filtration) so that the fibers are electrically pre-charged. But it is equally susceptible to particle loading and the fibers lose their electrical charge over time. Although powered air-purifying respirators can circumvent the breathing resistance caused by mechanical and electret filters by using a large motorized air blower, they are exceedingly bulky and noisy. At this juncture, it is important to highlight the fact that non-usage of a respirator (due to discomfort) could result in increased patient-to-patient transmission in a crowded environment, such as an emergency room

* Corresponding authors.
E-mail addresses: parkmr2140@gmail.com (M. Park), ahjeong.son@gmail.com, ason@ewha.ac.kr (A. Son), chuabeelee@gmail.com, bchua@korea.ac.kr (B. Chua).

https://doi.org/10.1016/j.snb.2018.08.133
Received 24 April 2018; Received in revised form 10 August 2018; Accepted 26 August 2018
Available online 29 August 2018

[21].

Inspired by industrial electrostatic precipitators, and borrowing from our prior work on their miniaturization, we investigated the feasibility of a microorganism-ionizing respirator (MIRI) [22–33]. This would be intended as a low breathing resistance alternative to existing mechanical filtration based personal respirators. Electrostatic precipitators are well known for their use in removing airborne particles, with efficiencies exceeding 90% [22–28]. Even in their miniaturized form, they have been shown to effectively capture airborne particles and microorganisms [29–33]. In particular, a miniaturized corona ionizer with pin cathode and liquid anode was used as a bio-precipitator to charge, capture, and lyse airborne bacteria prior to detection [33]. However the use of liquid anode only allows it to operate for a short duration (~1 min). In this work, MIRI employs a miniaturized corona ionizer with pin cathode and metallic anode to electrically charge the incoming airborne microorganisms, which are then captured downstream by a pair of separator electrodes. In addition, it uses manganese (IV) oxide coated mesh to remove excess ozone generated by the miniaturized corona ionizer. Since the airflow would be relatively unimpeded, compared to using mechanical filtration, the differential pressure (hence breathing resistance) would also be reduced.

In this study, we present two MIRI designs: MIRI-1 is designed for fitting over commercial facepieces, and MIRI-2 is designed with a custom facepiece. First, we will present the design and principle of operation. This is followed by an estimation of analytical airborne particle removal efficiency. Experimental measurements of the corona current versus applied voltage were performed for the miniaturized corona ionizer. The differential pressure across MIRI-1 was experimentally measured and compared with a commercial N95 respirator (Model 9322 K, 3 M, Paul, MN, USA), and a control (unobstructed flow). The ozone removal efficiency of the manganese (IV) oxide coated mesh (subsequently referred to as MnO mesh), was also experimentally characterized and compared against US-EPA's safety standard for ozone inhalation. Finally, the airborne bacterial removal efficiency was demonstrated for varying airflow rates. This was performed by using plate counting to monitor the amount of airborne bacteria removed by MIRI-1 and MIRI-2.

2. Materials and methods

2.1. Design and principle of operation

As shown in Fig. 1a and b, MIRI-1 consists of a miniaturized corona ionizer (pin-to-plane configuration), two pairs of separator electrodes, and two sets of manganese (IV) oxide coated mesh. The miniaturized corona ionizer further consists of a pin cathode (stainless steel, diameter ~50 μm) and a plane anode (aluminum shim, 8 mm × 3 mm), with an electrode gap of ~2 mm. The separator electrodes consist of two parallel planes (aluminum shim ~25 mm × 25 mm × 0.5 mm) with a gap of ~3 mm. The MnO mesh in the ozone removal stage consists of a folded steel mesh (thickness ~0.45 mm, mesh pore size ~1.6 mm × 1.3 mm) coated with manganese (IV) oxide powder (70%, Atom Scientific, Manchester, UK). There were two MnO mesh designs: Design A with 4 orthogonal folds, and Design B with 7 orthogonal folds (Fig. S1). The body of MIRI-1 was 3D printed with polylactic acid (Model CubePro, 3D Systems, Rock Hill, CA, USA) and the components were fastened with screws. A high voltage DC-DC converter (Model Q20N-5, EMCO, Chico, CA, USA) was positioned below the miniaturized corona ionizer in a separate compartment. An air inlet cover was used to prevent the user accidentally making contact with the corona ionizer.

The design of MIRI-2 was similar to MIRI-1. Its miniaturized corona ionizer used a pin-to-curve instead of a pin-to-plane configuration (Fig. S1). It also had a different MnO mesh design (Design C with 2 transverse folds). MIRI-2 also had a built-in fan to facilitate airflow (Model MF15B-05, SEPA Europe GmbH, Eschbach, Germany). The key dimensions of MIRI-1 and MIRI-2 are summarized in Table 1.

As shown in Fig. 2a–c, MIRI-1 was attached externally to a modified commercial facepiece. Note that the modified commercial facepiece was essentially an N95 respirator (Model 9322 K, 3 M) with the valve flap and valve cover removed to expose the valve opening. MIRI-1 was then fitted over the valve opening. In this way, most of the air entered via MIRI-1. On the other hand, MIRI-2 was attached internally to its own custom facepiece. Fig. 2d shows the interior of MIRI-2 with the back cover and MnO mesh removed. The characteristic glow of the miniaturized corona ionizer can be observed from the rear, via the air outlet (Fig. 2d and e). Fig. 2f shows the photo of the miniaturized corona ionizer used in MIRI-2. It has the similar footprint to a 8 pin integrated circuit dual inline package and can be plugged in or removed easily. Fig. 2g and h shows the photo and electron micrographs (SNE-3000MS, SEC, Suwon, Korea) of the MnO mesh (Design A).

During operation, air laden with microorganisms entered via the air inlet and flowed past the miniaturized corona ionizer. The electron and gas ion cloud, generated by the corona ionizer, electrically charged the airborne microorganisms. As the charged airborne microorganisms entered the electric field of the separator electrodes, they acquire a drift velocity that was orthogonal to the airflow. The charged microorganisms were captured as they drifted toward, then made contact with, the separator electrodes. As the miniaturized corona ionizer also generated ozone, the excess ozone in the airflow was removed by the MnO mesh (by the following decomposition equations) prior to exiting through the air outlet [34].

$$O_3 + * \rightarrow O_2 + O^* \tag{1a}$$

$$O_3 + O^* \rightarrow O_2 + O_2^* \tag{1b}$$

$$O_2^* \rightarrow O_2 + * \tag{1c}$$

2.2. Analytical airborne particle removal efficiency

Assuming the airborne particles acquired saturation charge via combined charging, the particle saturation charge is given by [35,36]

$$Q_p^{\infty} = \left\{(1 + K_n)^2 + \left(\frac{2}{1 + K_n}\right)\left(\frac{\varepsilon_r - 1}{\varepsilon_r + 2}\right)\right\}\pi\varepsilon_o d_p^2 E_I \tag{2}$$

where $Q_p{}^{\infty}$ is the particle saturation charge, K_n is the Knudsen number given by $2\lambda/d_p$, $\lambda = 65$ nm is the air mean free path at 298 K and 1 atm, d_p is the particle diameter, $\varepsilon_r = 2$ is the electrical permittivity of the particle (conservative estimate), $\varepsilon_o = 8.85 \times 10^{-12}$ F/m is the electrical permittivity of free space, and E_I is the electric field between the cathode and anode of the corona ionizer.

Given the particle's charge from Eq. (2), the particle's drift velocity is calculated as follows [36,37]:

$$V_{drift} = \frac{Q_p{}^{\infty} C_c E_s}{3\pi\mu d_p} \tag{3}$$

where $\mu = 1.8 \times 10^{-5}$ kg/m/s is the dynamic viscosity of air at 298 K and 1 atm, E_s is the electric field of the separator electrodes, and C_c is the Cunningham slip coefficient that in turn is given by $C_c = 1 + 1.647\ K_n$ [38].

The analytical airborne particle removal efficiency $R_{eff\text{-}analytical}$ is calculated using a similar scheme to Chua et al., and is given by [32]

$$R_{eff-analytical} = \frac{V_{drift}\tau}{X_{SE}} \tag{4a}$$

$$\tau = \frac{U_{air}}{Y_{SE}} \tag{4b}$$

where X_{SE} is the electrode spacing of the separator electrodes, Y_{SE} is the length of the separator electrodes, τ is the airborne particle residence time between the separator electrodes, and U_{air} is the airflow velocity

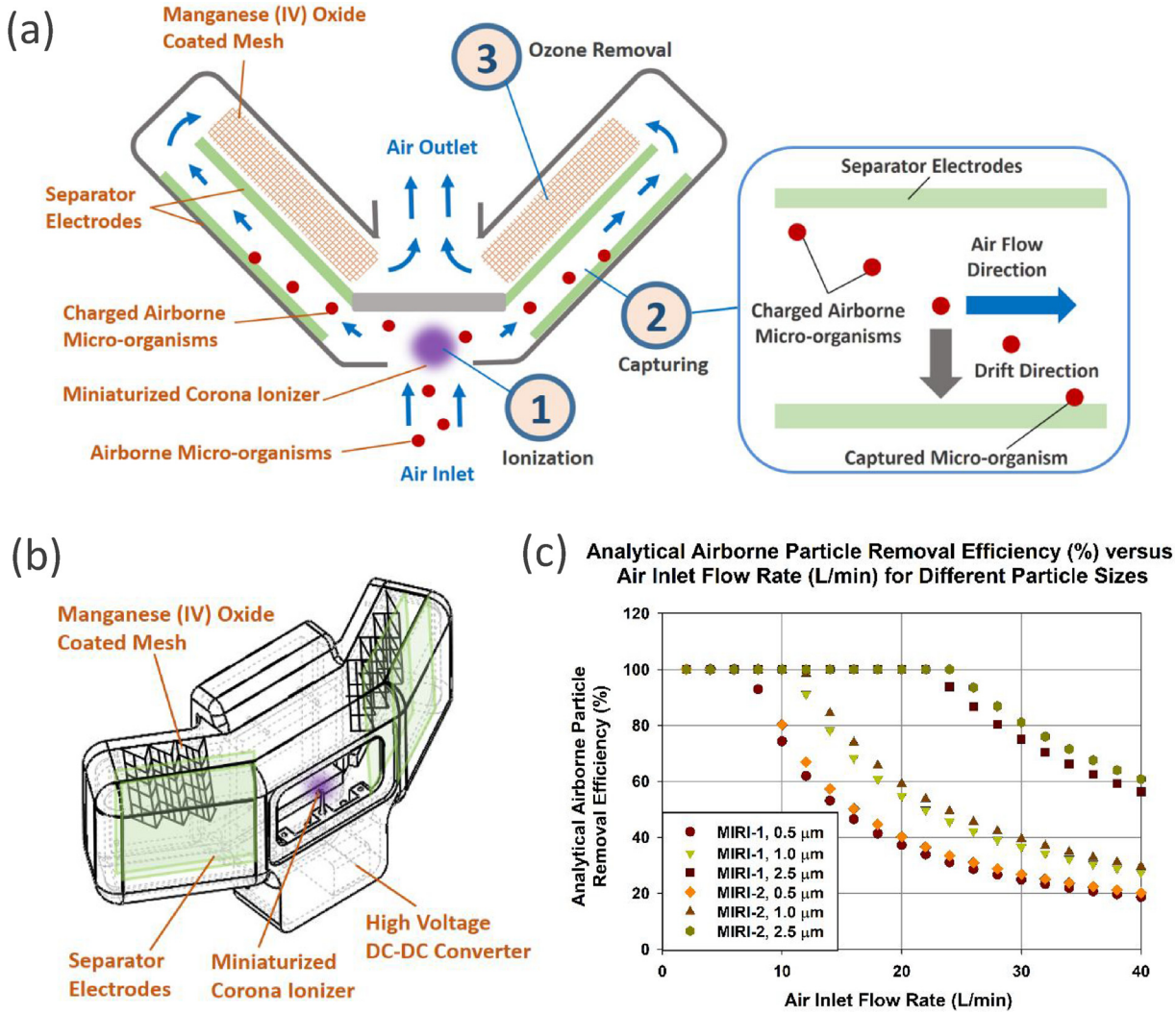

Fig. 1. (a) Top-view operational schematic of MIRI-1. (b) 3D schematic of MIRI-1. (c) Analytical airborne particle removal efficiency (%) versus air inlet flow rate (L/min) for different particle sizes using MIRI-1 and MIRI-2.

Table 1
Dimensions of miniaturized corona ionizer, separator electrodes and ozone removal stage for MIRI-1 and MIRI-2.

	MIRI-1	MIRI-2
Corona Ionizer Configuration	Pin-to-Plane	Pin-to-Curve
Corona Ionizer Gap	~2.0 mm	~2.0 mm
Corona Ionizer Cathode Diameter	~50 μm	~50 μm
Corona Ionizer Anode Length	8 mm	–
Corona Ionizer Anode Height	3 mm	5 mm
Separator Electrodes Length	25 mm	18 mm
Separator Electrodes Height	25 mm	40 mm
Separator Electrodes Gap	3 mm	5 mm
Ozone Removal Stage Length	25 mm	20 mm
Ozone Removal Stage Height	25 mm	40 mm
Ozone Removal Stage Gap	7 mm	7 mm

(given by the air inlet flow rate divided by the cross-sectional area of the space between the separator electrodes).

The applied voltages for the corona ionizer (the same as for the separator electrodes) for MIRI-1 and MIRI-2 were 1600 and 2000 V, respectively. The same settings were used in the subsequent experiments, unless otherwise stated.

Using airborne particle sizes (diameter) of 0.5, 1.0, and 2.5 μm, the removal efficiency (%) was calculated for air inlet flow rates from 0 to 40 L/min. As shown in Fig. 1c, the removal efficiencies for both MIRI-1 and MIRI-2 are similar. At an air flow rate of 24 L/min (adult male walking at 2.5 mph) [39], the MIRI-1 removal efficiencies for 0.5, 1.0, and 2.5 μm particles were ~31%, 46%, and 94%, respectively. Similarly, the MIRI-2 removal efficiencies for 0.5, 1.0, and 2.5 μm particles were ~33%, 49%, and 100%, respectively. At an air flow rate of 10 L/min (adult male sitting/standing), the MIRI-1 removal efficiencies for 0.5, 1.0, and 2.5 μm particles increased to ~74%, 100%, and 100%, respectively. Similarly, the MIRI-2 removal efficiencies for 0.5, 1.0, and 2.5 μm particles also increased to ~80%, 100%, and 100%, respectively.

2.3. Experimental corona current versus applied voltage measurement

The miniaturized corona ionizers employed in MIRI-1 (pin-to-plane configuration) and MIRI-2 (pin-to-curve configuration) were electrically characterized using a bench top high voltage variable power supply (Model PS 350, Stanford Research Systems Inc, Sunnyvale, CA, USA). The applied voltage was varied from 1600 to 2600 V, in steps of 100 V. At each applied voltage, the corresponding corona current was observed from the high voltage variable power supply and recorded. All measurements were performed three times, unless otherwise stated.

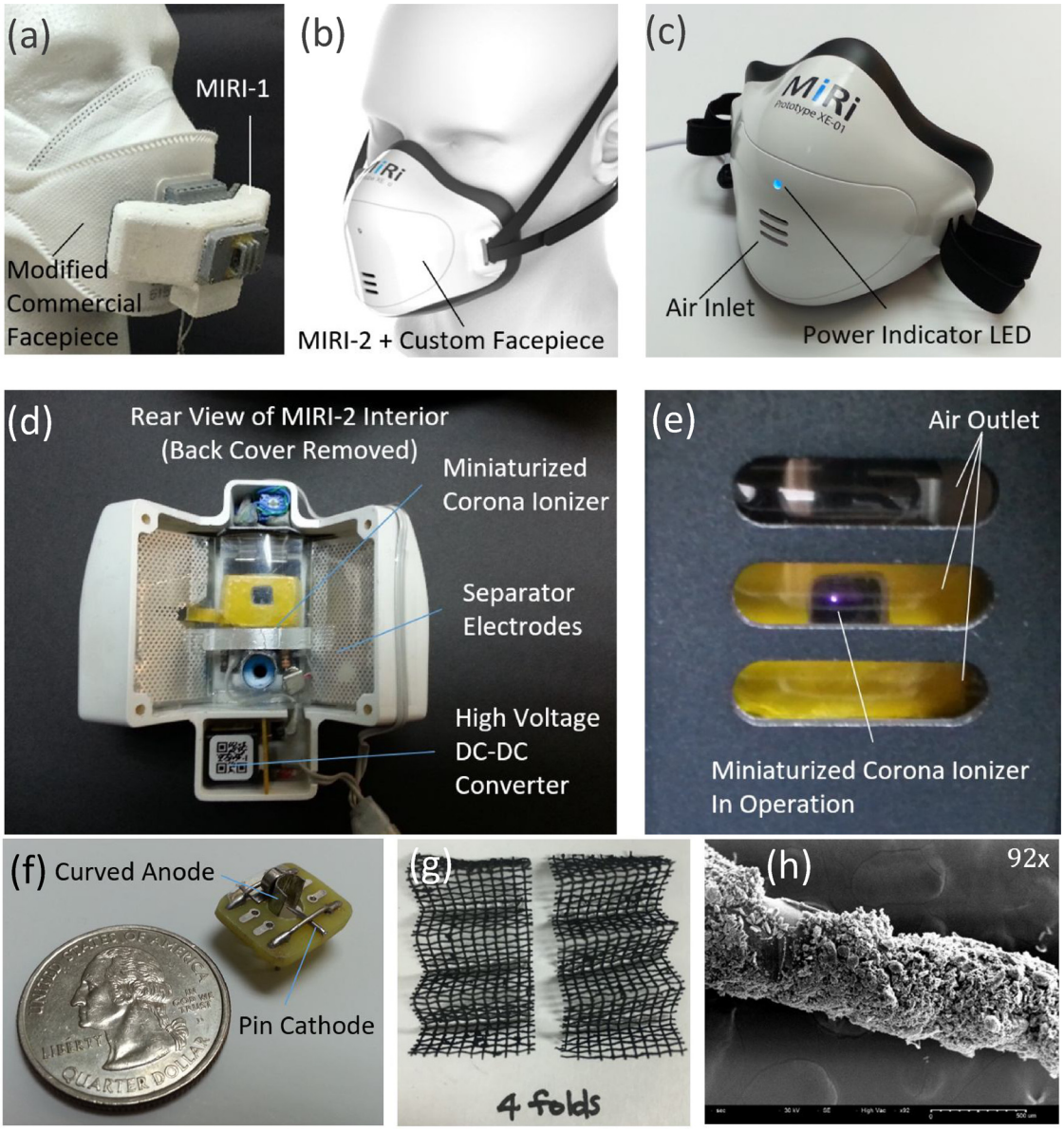

Fig. 2. (a) Photo of MIRI-1 fitted over a modified commercial facepiece. (b) Model of MIRI-2 with its custom facepiece. (c) Photo of MIRI-2 with its custom facepiece and power indicator LED light. (d) Rear view photo of MIRI-2s interior (manganese (IV) oxide coated mesh and back cover are removed). (e) Rear view photo (via the air outlet) of MIRI-2 miniaturized corona ionizer in operation with its distinctive glow. (f) Photo of MIRI-2 miniaturized corona ionizer. (g) Photo of the manganese oxide (IV) coated mesh – Design A. (h) SEM images of a manganese oxide (IV) coated mesh at 92× of magnification.

2.4. Experimental differential pressure measurement

As shown in Fig. 3a, the experimental differential pressure measurement setup consists of a mannequin head attached to an air flow column (~80 mm diameter). This is connected to an exhaust fan (Model Gamma29 D09F-12BS1 09, Nidec Corporation, Japan) powered by a variable DC power supply (Model HY3005F-3, Mastech, China). As mentioned earlier, MIRI-1 was attached to a modified commercial facepiece. The pressure drop across MIRI-1 was measured via a differential manometer (Model GM510, Benetech, China), with one end inside the facepiece and the other at atmospheric pressure. During the experiment, the exhaust fan was powered at 9, 12, and 15 V. The corresponding average flow velocities (hence approximate flow rates) for each setting were measured using an anemometer (Model T8, Benetech, China). The differential pressure and corresponding flow rate of MIRI-1 were compared to that of a commercial N95 respirator, as well as a control (unobstructed flow). Each measurement was repeated three times.

2.5. Experimental ozone removal measurement by manganese (IV) oxide coated mesh

As shown in Fig. 3b, the ozone removal measurement setup consists of the in-line arrangement of an air inlet fan (Model MF15B-05, SEPA Europe GmbH, Eschbach, Germany), MIRI-1, and an ozone sensor (Model A22, EcoSensors, Newark, CA, USA). During the experiment, a variable DC power supply (Model HY3005F-3, Mastech, China) powered both the air inlet fan and the high voltage DC-DC converter of MIRI-1. The air inlet fan was operated from 3 to 9 V, with 1 V increments. This corresponded to air flow rates from 12 to 27.6 L/min, as measured by an anemometer (Model GM8903, Benetech, China). Note that these flow rates also corresponded to the breathing rate of an adult male standing and walking (2.5 mph) [39,40]. The air entered MIRI-1 via the air inlet, and ozone was produced as a by-product of the corona

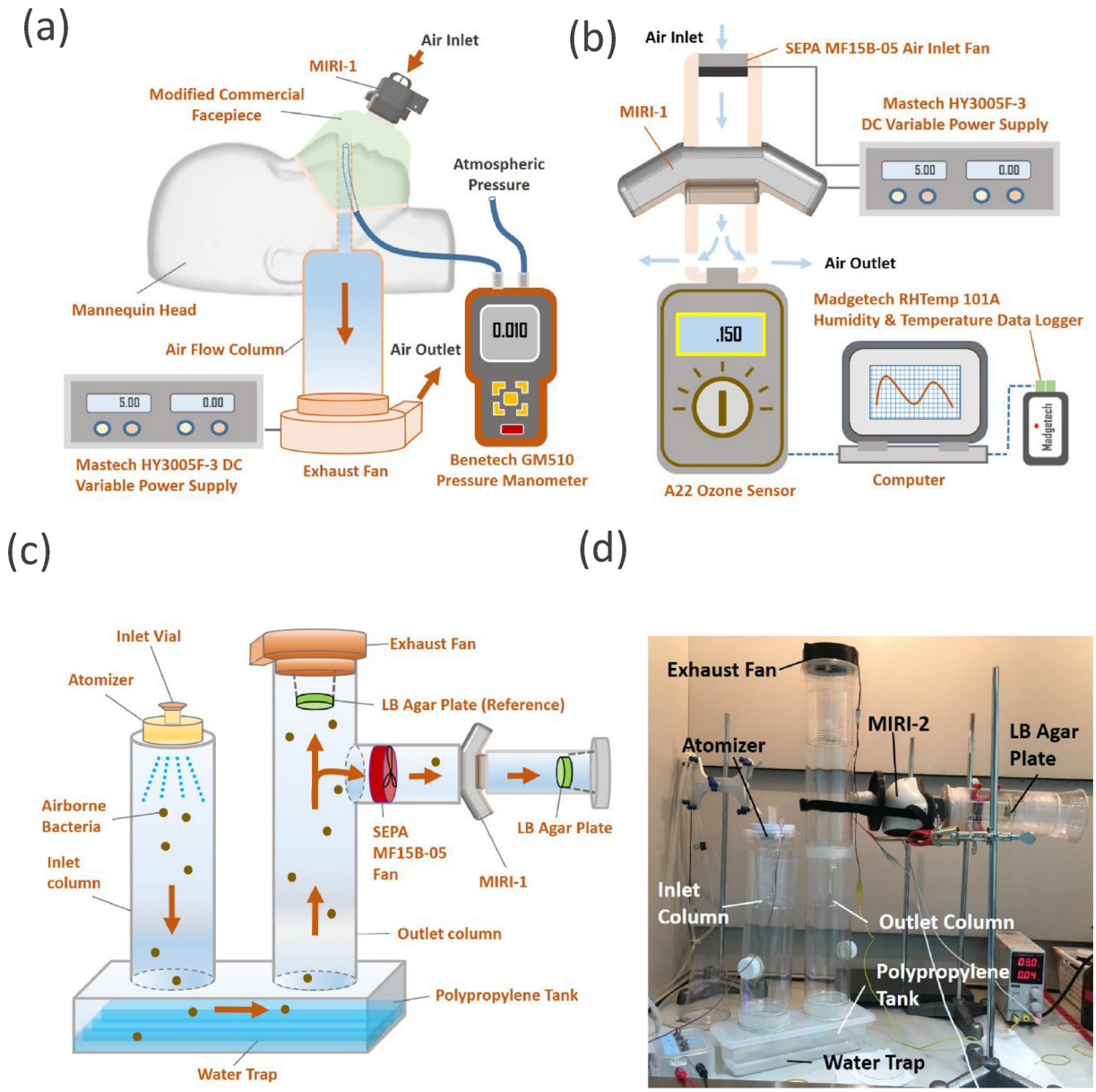

Fig. 3. Schematic of the experimental setup for (a) pressure drop measurement for MIRI-1, (b) ozone measurement for MIRI-1, and (c) airborne bacteria exposure test for MIRI-1. (d) Photo of airborne bacteria exposure test for MIRI-2.

ionizer. As mentioned earlier, the ozone in the air flow was reduced as it flowed past the MnO mesh in the ozone removal stage. MnO mesh designs A and B were used in the experiment. Prior to exiting the air outlet, the ozone sensor measured the ozone concentration in the air flow. The data sampling rate was two readings/sec. At the beginning of the experiment (at a particular flow rate), a 1 min average measurement was used as the baseline ozone concentration. Then the ozone concentration was allowed to increase for 45 min, until it reached a steady state. The average steady-state ozone concentration was obtained over the next 10 min. The final ozone concentration was deduced by subtracting the baseline ozone concentration from the steady-state ozone concentration. The experiment was performed at ~25 °C and RH of < 30% (monitored by Model RHTemp101A humidity and temperature data logger, MadgeTech, Warner, NH, USA). Note that a similar experimental setup was also used to characterize MIRI-2. In this case, MnO mesh design C was used.

2.6. Experimental airborne bacterial removal efficiency

Escherichia coli K12 (*E. coli* K12, ATCC 10798, Manassas, VA, USA) was selected as the target bacteria for the experiment. *E. coli* K12 is a Gram-negative bacteria and has a rod shape (diameter: 0.3–1.0 μm; length: 1–6 μm). *E. coli* K12 was cultured in 50 mL of LB broth (Difco-BD, Frankin Lakes, NJ, USA) at 37 °C in a shaking incubator (WIS-30R, Wisecube, Korea) at 180 rpm. The cell concentration of *E. coli* K12 was measured by a commercial spectrofluorometer (SpectraMax M2, Molecular Devices, Sunnyvale, CA, USA) at 600 nm. Prior to the experiment, cultured *E. coli* K12 was centrifuged at 4500 rpm for 20 min, and washed twice with deionized water. Three-fold serial dilution was performed with 0.1 mol/L phosphate buffered saline (PBS, pH 7.4), and the final bacterial concentration in the atomization solution was 2.1×10^8 CFU/L (CFU: Colony forming unit).

As shown in Fig. 3c, the experimental setup is similar to that employed by Lee et al. [33]. It consists of an inlet vial positioned over an atomizer, a U-shape exposure chamber, and an exhaust fan (Model Gamma29 D09F-12BS1 09, Nidec Corporation, Japan). The U-shaped

exposure chamber further consists of inlet and outlet columns (polyethylene terephthalate, diameter ~80 mm, heights ~320 and 580 mm, respectively), and a polypropylene tank as a water trap. The exhaust fan located on top of the outlet column was powered at 3 V, with a corresponding flow rate of ~135 L/min (using average flow velocity measured by an anemometer, Model T8, Benetech). A reference LB agar plate was positioned just before the exhaust fan, to monitor the viability of the airborne bacteria. The inlet fan was operated at 3, 6, and 9 V (corresponding to currents of 40, 60, and 70 mA, respectively). This corresponded to flow rates of 12, 19.8, and 27.6 L/min.

During the experiment, 300 µL of the atomization solution was pipetted into the inlet vial. The airborne bacteria was diverted from the outlet column into MIRI-1, via the inlet fan. The airborne bacteria exiting MIRI-1 was detected via a LB agar plate (Difco-BD) positioned downstream. MIRI-1 was powered on and off for each setting, and PBS was used as a negative control. All experiments were performed in triplicate, at a temperature of ~28 °C and RH of ~60%. The total running time was 3 min. Between each run, 300 µL of deionized water was pipetted into the inlet vial and allowed to run for 1 min.

The experimental airborne bacteria concentration could be approximated by dividing the total bacterial count in the atomization solution, by the total volume of air flowed during the running time, and was calculated as $\sim 1.6 \times 10^5$ CFU/m^3. Note that this order of magnitude ($\sim 10^5$ CFU/m^3) is also environmentally relevant [41]. After each run, the LB agar plate was incubated at 37 °C overnight, and the incubated colonies were counted by CFU counting. Five runs were performed for each setting. Negative control was obtained with deionized water as an atomization solution. As shown in Fig. 3d, a similar experimental setup was also used to characterize the experimental airborne bacterial removal efficiency for MIRI-2.

3. Results and discussion

3.1. Experimental corona current versus applied voltage measurement

As shown in Fig. 4a, the experimental corona current for the miniaturized corona ionizer in MIRI-1 increased from ~3 to 33 µA, as the applied voltage increased from 1600 to 2600 V. Similarly, the experimental corona current for MIRI-2 increased from ~4 to 55 µA, as the applied voltage increased from 1800 to 2600 V. The steeper gradient associated with MIRI-2 may be attributed to the pin-to-curve configuration of its corona ionizer.

At an applied voltage of 1600 V, and an experimental corona current of 3 µA, the power required to operate MIRI-1's corona ionizer was ~4.8 mW. On the other hand, MIRI-2 was operated at 2000 V, with an experimental corona current of 21 µA, and the power required to operate its corona ionizer was ~41 mW. Assuming the high voltage DC-DC converter efficiency of 50% and maximum inlet fan flow rate (9 V at 70 mA, 630 mW), the power consumption for MIRI-1 and MIRI-2 were ~640 and 710 mW, respectively.

3.2. Experimental differential pressure measurement

As shown in Fig. 4b, MIRI-1 exhibited higher flow rates at lower differential pressures compared to an N95 respirator. With the exhaust fan powered at 9 V (dotted box in Fig. 4b), air flowed through the N95 respirator at ~195 L/min, with a differential pressure of ~21 Pa. For the same exhaust fan voltage, MIRI-1 had a higher flow rate of ~210 L/min, with a lower differential pressure of ~14 Pa. For comparison, the control (unobstructed flow) yielded the highest flow rate of ~225 L/min, at the lowest differential pressure of ~7 Pa. In other words, the flow resistance of the N95 respirator, MIRI-1, and control (unobstructed flow) were ~0.11, 0.07, and 0.03 Pa/L/min, respectively. This means the flow resistance of MIRI-1 was ~50% of an N95 respirator.

Similar trends were also observed at higher exhaust fan voltages of 12 and 15 V. At an exhaust fan voltage of 12 V, the N95 respirator, MIRI-1, and control (unobstructed flow) yielded ~248 L/min at ~40 Pa, ~263 L/min at ~14 Pa, and ~278 L/min at ~ 7 Pa, respectively. At an exhaust fan voltage of 15 V, the N95 respirator, MIRI-1, and control (unobstructed flow) yielded ~290 L/min at ~53 Pa, ~303 L/min at ~21 Pa, and ~330 L/min at ~14 Pa, respectively. In this case, the flow resistance for the N95 respirator, MIRI-1, and control (unobstructed flow) were ~0.18, 0.07, and 0.04 Pa/L/min, respectively. This means the flow resistance of MIRI-1 was ~40% of an N95 respirator. Therefore MIRI-1 (and conceivably MIRI-2) should significantly improve the user's ease of breathing, compared to an N95 respirator.

3.3. Experimental ozone removal measurement by manganese (IV) oxide coated mesh

As shown in Fig. 4c, without the MnO mesh, the ozone concentration in the air flow exited from MIRI-1 ranged from 0.340 ± 0.025 to less than 0.010 ppm. The flow rates ranged from 12 to 27.6 L/min. With MnO mesh (Design A), the maximum ozone concentration (for the same range of flow rates) was reduced to 0.144 ± 0.004 ppm (at a flow rate of 19.8 L/min). With MnO mesh (Design B), the maximum ozone concentration was further reduced to 0.023 ± 0.007 ppm (at a flow rate of 17.2 L/min).

Similarly for MIRI-2 (Fig. 4d), without the MnO mesh, the ozone concentration ranged from 0.331 ± 0.009 to 0.078 ± 0.003 ppm. With MnO mesh (Design C), the maximum ozone concentration was reduced to 0.117 ± 0.002 ppm (at a flow rate of 14.6 L/min).

At an air inlet flow rate of 27.6 L/min, the ozone concentration in the MIRI-1 outlet flow was below 0.010 ppm, for both MnO mesh designs. At the same flow rate, the ozone concentration in the MIRI-2 outlet flow was 0.032 ± 0.006 ppm. In both cases, the ozone concentration was below the threshold of 0.1 ppm, as stipulated by the Occupational Safety and Health Administration (OSHA PEL – General Industry 29 CFR 1910.1000 Table Z-1). This means both MIRI-1 and MIRI-2 could be worn safely by an adult (male or female) walking at 2.5 mph (breathing rate of 24.10 and 20 L/min, respectively), and by children playing outdoors (breathing rate of 17.5 L/min).

3.4. Experimental airborne bacterial removal efficiency

As expected, the negative control (with deionized water as atomization solution) yielded no CFU (Fig. S2), and the reference LB agar plates showed viable CFUs (Fig. S3). Fig. 5a and b show photo representations of both MIRI-1 and MIRI-2 airborne bacteria removal efficiencies. The complete set of LB agar plate photos from the experiment are shown in Figs. S4 and S5. For both MIRI-1 and MIRI-2 in operation (with the miniaturized corona ionizer and separator electrodes switched on), it is apparent from the photos that the number of colonies were visibly less for all three flow rates. This means that less airborne bacteria were able to flow through MIRI-1 and MIRI-2 when they were in operation.

As shown in Fig. 6a, where MIRI-1 was not in operation and at flow rate of 12.0 L/min, the average CFU was 1322 ± 387 CFU/plate. When it was in operation at the same flow rate, the average CFU was reduced to 171 ± 66 CFU/plate. At the higher flow rate of 19.8 L/min, the average CFUs were 2549 ± 546 (not in operation), and 612 ± 284 CFU/plate (in operation). Finally, at a flow rate of 27.6 L/min, the average CFUs were 2650 ± 783 (not in operation), and 513 ± 240 CFU/plate (in operation).

Similarly, for MIRI-2 (Fig. 6b), at a flow rate of 12.0 L/min, the average CFUs were 30 ± 47 (not in operation) and 0 CFU/plate (in operation). At a flow rate of 19.8 L/min, the average CFUs were 1239 ± 123 (not in operation), and 197 ± 150 CFU/plate (in operation). Finally, at the flow rate of 27.6 L/min, the average CFUs were 2238 ± 538 (not in operation), and 787 ± 499 CFU/plate (in operation).

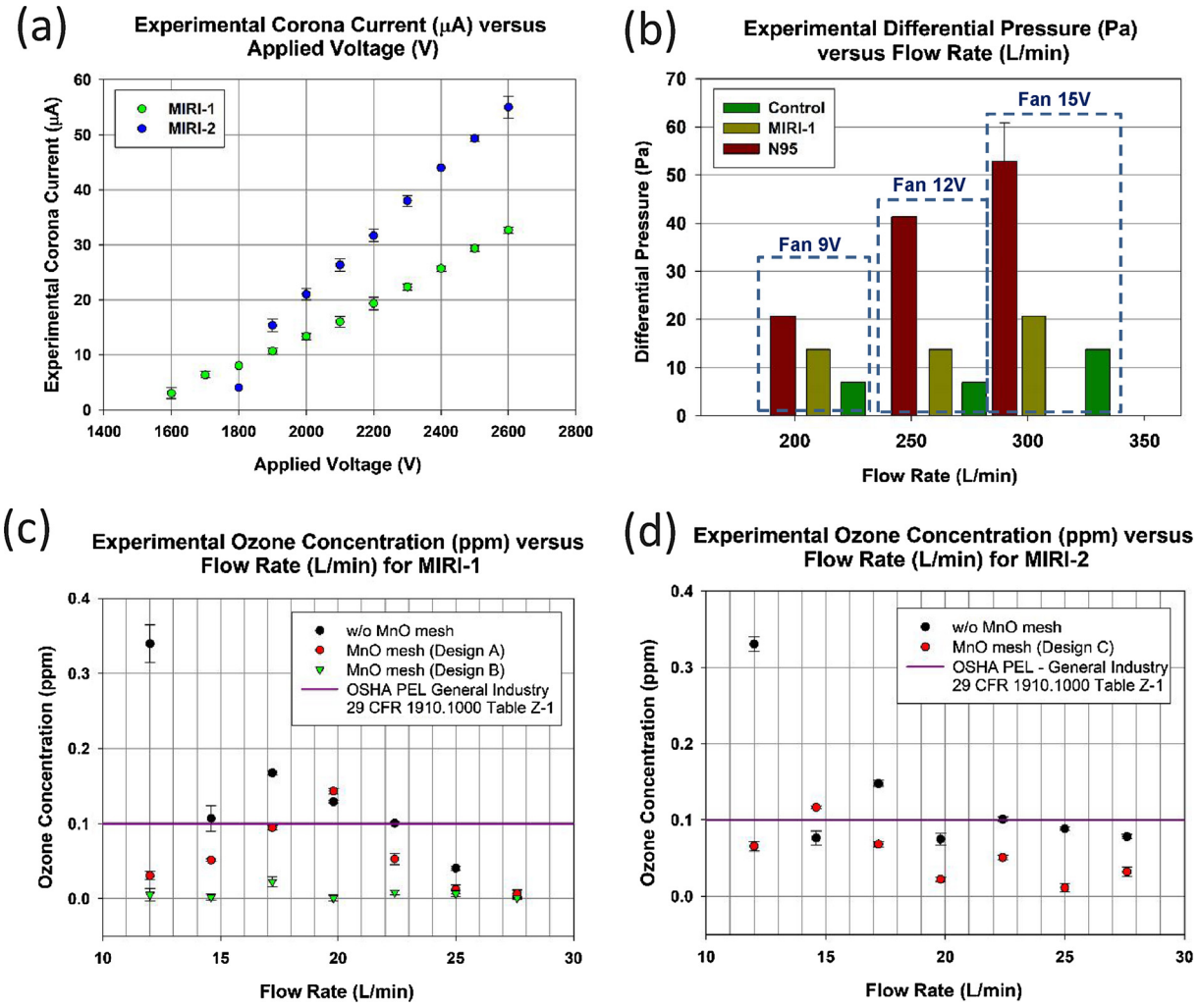

Fig. 4. (a) Experimental corona current (μA) versus applied voltage (V). (b) Experimental differential pressure (psi) versus flow rate (L/min). (c) Experimental ozone concentration (ppm) versus flow rate (L/min) for MIRI-1. (d) Experimental ozone concentration (ppm) versus flow rate (L/min) for MIRI-2.

The experimental airborne bacterial removal efficiency $R_{eff\text{-}experimental}$ was calculated as follows:

$$R_{eff-experimental} = average\left(\frac{CFU_{not\ \ in\ \ operation} - CFU_{in\ \ operation}}{CFU_{not\ \ in\ \ operation}}\right) \quad (5)$$

As shown in Fig. 6c, the experimental airborne bacterial removal efficiencies for MIRI-1, at flow rates of 12.0, 19.8, and 27.6 L/min, were ~85%, 75%, and 79%, respectively. As shown in Fig. 6d, the experimental airborne bacterial removal efficiencies for MIRI-2, at flow rates of 12.0, 19.8, and 27.6 L/min, were ~100%, 85%, and 65%, respectively. Note that the experimental airborne bacteria removal efficiencies for both MIRI-1 and MIRI-2 were within the analytical range, as shown in Fig. 1c.

3.5. Significance and limitations

As mentioned earlier, the breathing rate of ~20 L/min corresponds to an adult walking at 2.5 mph. In this situation, MIRI-1 and MIRI-2 could operate with ~75% and 85% airborne bacteria removal efficiency, respectively. For an adult standing or sitting (breathing rate of ~10 L/min or less) [39,40], MIRI-1 and MIRI-2 could operate with ~85% and 100% airborne bacterial removal efficiency, respectively. It is important to note that the above mentioned airborne bacterial removal efficiencies were accompanied by a significant reduction in breathing resistance. Furthermore, it is conceivable that the airborne bacterial removal efficiency could be further increased by extending the separator electrodes into the ozone removal stage.

The power consumption of both MIRI-1 and MIRI-2 were ~640 and 710 mW, respectively. Using a commercial portable pocket size power bank of ~50,000 mA h (250,000 mW h at 5 V), both MIRI-1 and MIRI-2 could be powered for over 350 h, which is over 2 weeks of continual use.

Given the airborne bacterial removal efficiency (~75%–100%), significant reduction in breathing resistance (more than 50%), and ability to be powered for long durations by a pocket-sized power bank (more than 2 weeks), both MIRI-1 and MIRI-2 could be useful in a number of scenarios. Note that the differential pressure measurements were performed at flow rates much higher (~200 L/min) than its intended flow rate range (~20 L/min). Therefore, the difference in breathing resistance at the intended flow rate range may be lower. Nonetheless, a fractional reduction in breathing resistance would still be useful and desirable. For example, it could be useful for a healthcare worker during an airborne pathogenic outbreak, such as tuberculosis. The healthcare worker would constantly be exposed to the pathogen while working with patients for an extended duration. Another example would be an elderly patient, with a compromised breathing capacity, waiting in a crowded emergency room while exposed to potential airborne pathogens. In both scenarios, a reduction in breathing resistance, with the accompanied portability, would be highly desirable.

A potential limitation of this approach pertains to the corrosion of

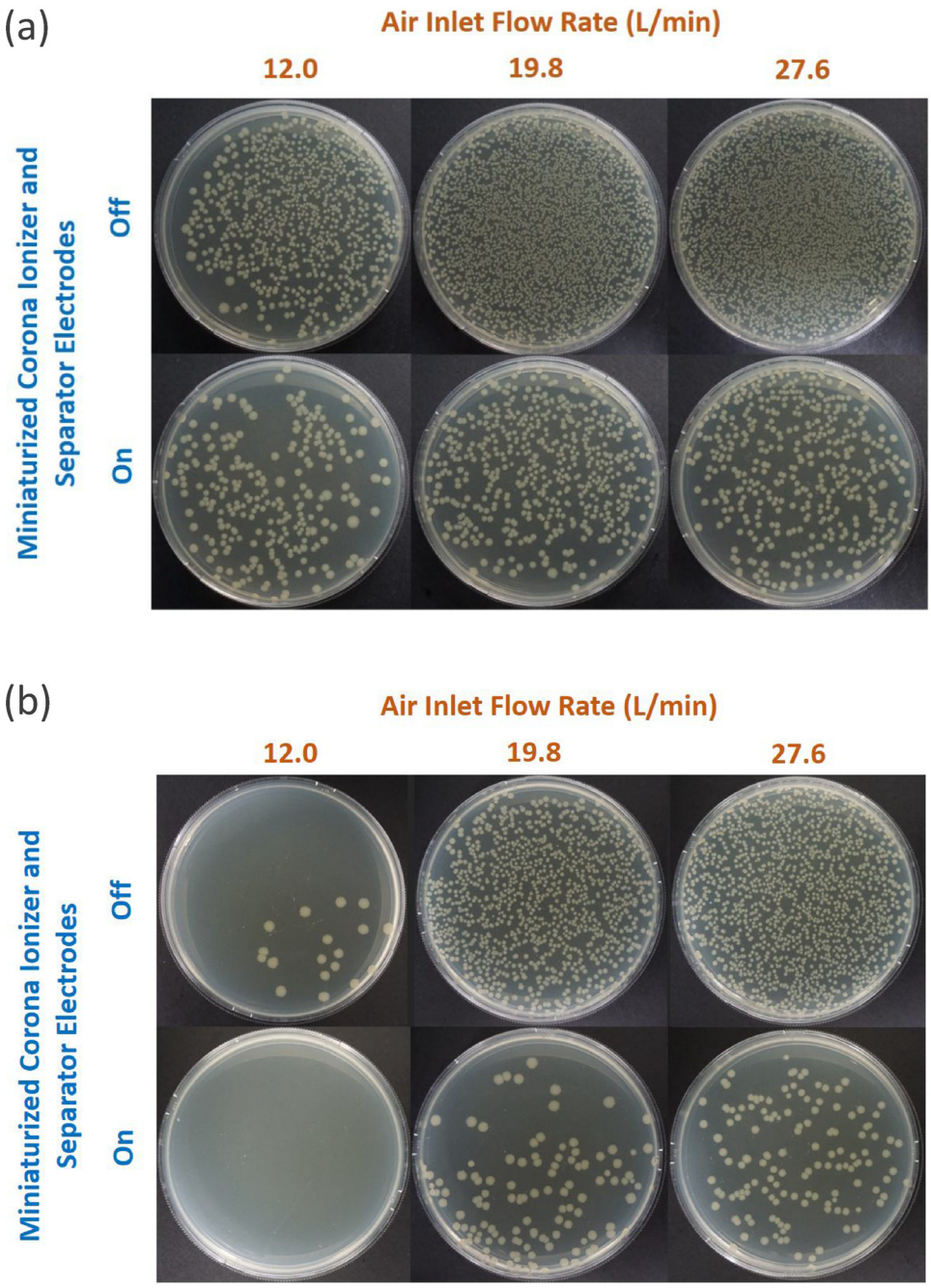

Fig. 5. Airborne bacteria exposure test with an atomizing solution concentration of 2×10^8 CFU/L for various flow rates (a) MIRI-1 (b) MIRI-2.

the electrodes of the miniaturized corona ionizer. Extended operation in a high humidity environment may accelerate the corrosion. This means that periodic replacement would be necessary. Furthermore, the separator electrodes would also need to be cleaned or replaced periodically. Another limitation of this approach relates to the possible re-entrainment of MnO powder from the mesh, and hence into the air flow. This could be circumvented by using a more durable coating, or by forming techniques such as the hydrothermal method [42]. In addition, this feasibility study was only performed on bacteria. Though it is reasonable (and tempting) to extend the usage to other airborne microorganisms, such as viruses and spores, it would be necessary to repeat the experiment with other airborne microorganisms in the future. In the case of person-to-person airborne transmission of viruses, it is concievable that they are also transmitted via larger respiratory droplets. Finally, there is an absence of on-board bacterial detection mechanism although it may be possible to analyze the captured microorganisms separately via existing bacterial detection methods [43,44].

In summary, we have demonstrated that it is possible to remove airborne bacteria using microorganism-ionizing respirators and their performance are summarized in Table S1. Both designs have demonstrated airborne bacterial removal efficiencies of ~75%–100%, for flow rates ranging from ~10 to 20 L/min. This range of flow rates corresponds to breathing rates for standing or walking adults. As no mechanical filtration was used, the breathing resistance of the microorganism-ionizing respirators were lower than that of a commercial N95 respirator. Finally, its low power consumption would imply that it could be powered by a portable power bank for an extended period of time (more than 2 weeks). Therefore, it would be useful for healthcare workers during an airborne pathogenic outbreak and for patients with

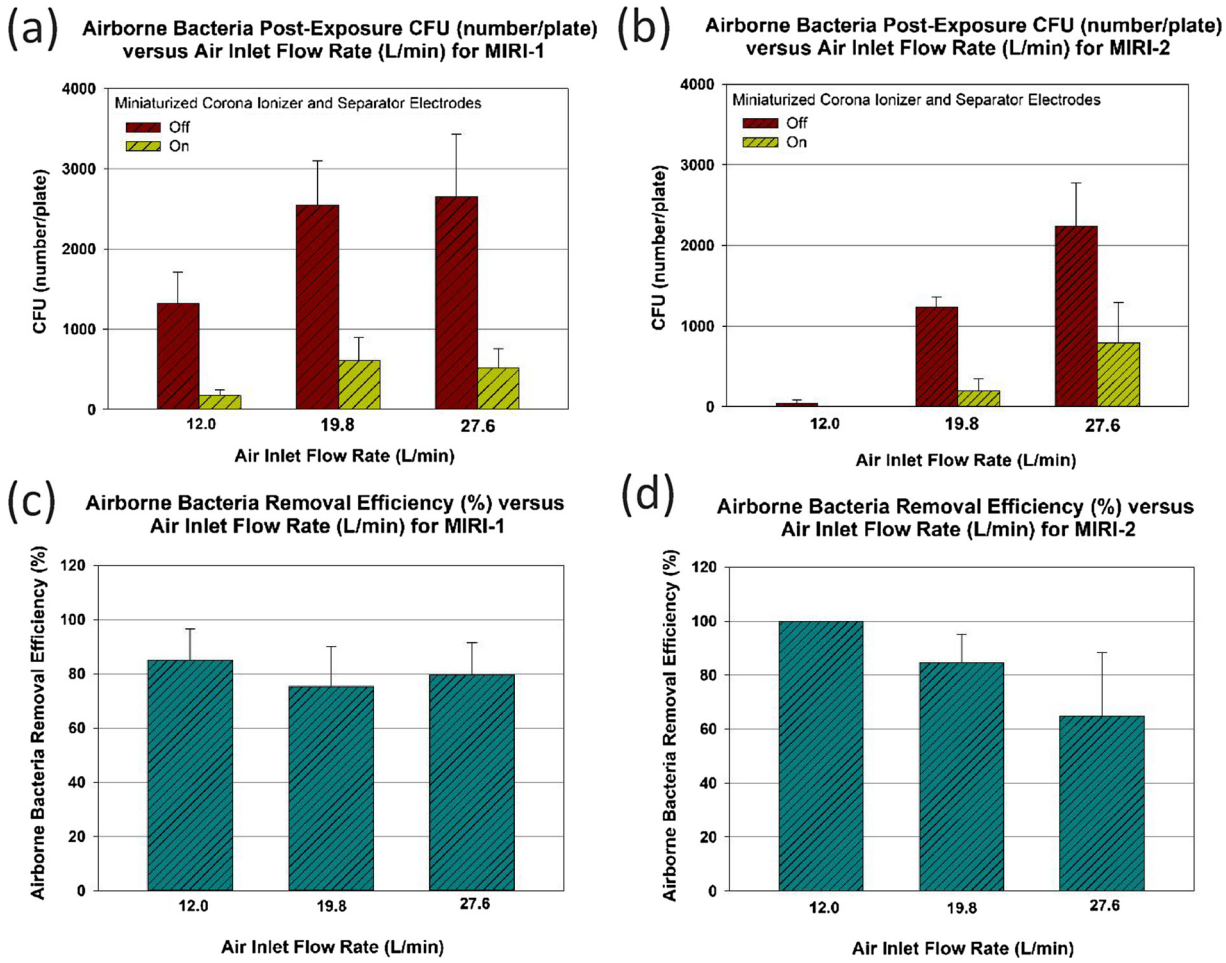

Fig. 6. Airborne bacteria post-exposure CFU (number/plate) versus air inlet flow rate (L/min) for (a) MIRI-1 (b) MIRI-2. Airborne bacteria removal efficiency (%) versus air inlet flow (L/min) for (c) MIRI-1 (d) MIRI-2.

compromised breathing capacity.

Acknowledgements

This work was supported by National Research Foundation of Korea (NRF-2017R1A2B4005133 and NRF-2015R1D1A1A01060317). The authors thank Prof. Yongpyo Kim for the discussions, and Hyowon Jin, Hebin Cho, and Juhyun Lee of Ewha Womans University, Seoul, Korea for their assistance in the agar plate counting experiments.

Appendix A. Supplementary data

Supplementary material related to this article can be found, in the online version, at doi:https://doi.org/10.1016/j.snb.2018.08.133.

References

[1] A. Trilla, G. Trilla, C. Daer, The 1918 “Spanish flu” in Spain, Clin. Infect. Dis. 47 (2008) 668–673.
[2] Centers for Disease Control and Prevention, Update: severe acute respiratory syndrome-worldwide and United States, 2003, MMWR Morb. Mortal. Wkly. Rep. 52 (2003) 664–665.
[3] M. Aly, M. Elrobh, M. Alzayer, S. Aljuhani, H. Balkhy, Occurrence of the Middle East Respiratory Syndrome Coronavirus (MERS-CoV) across the Gulf Corporation Council countries: four years update, PLoS One 12 (2017) e0183850.
[4] J. Park, K. Lee, K. Lee, S. Lee, J. Cho, J. Mo, et al., Hospital outbreaks of middle east respiratory syndrome, Daejeon, South Korea, 2015, Emerg. Infect. Dis. 23 (2017) 898–905.
[5] E. de Wit, N. van Doremalen, D. Falzarano, V.J. Munster, SARS and MERS: recent insights into emerging coronaviruses, Nat. Rev. Microbiol. 14 (2016) 523–534.
[6] A.E. Tozzi, L. Pastore Celentano, M.L. Ciofi degli Atti, S. Salmaso, Diagnosis and management of pertussis, CMAJ: Can. Med. Assoc. J. 172 (2015) 509–515.
[7] N.R. Adler, A. Mahony, N.D. Friedman, Diphtheria: forgotten, but not gone, Intern. Med. J. 43 (2013) 206–210.
[8] N. Fogel, Tuberculosis: a disease without boundaries, Tuberculosis 95 (2015) 527–531.
[9] World Health Organization, Pertussis vaccines, Wkly. Epidemiol. Rec. 74 (1999) 137–144.
[10] W. Cruz-Knight, L. Blake-Gumbs, Tuberculosis: an overview, Prim. Care 40 (2013) 743–756.
[11] World Health Organization, Tuberculosis Fact Sheet, WHO Global TB Programme, Geneva (Switzerland), 2014.
[12] E.R. Jane, D. Siegel, M. Jackson, L. Chiarello, The Healthcare Infection Control Practices Advisory Committee, 2007 Guideline for Isolation Precautions: Preventing Transmission of Infectious Agents in Healthcare Settings, (2007).
[13] S. Yang, G.W. Lee, C.M. Chen, C.C. Wu, K.P. Yu, The size and concentration of droplets generated by coughing in human subjects, J. Aerosol Med. 20 (2007) 484–494.
[14] Centers for Disease Control and Prevention (CDC), Interim Infection Prevention and Control Recommendations for Hospitalised Patients With Middle East Respiratory Syndrome Coronavirus, MERS-CoV, 2014.
[15] U.K. Public Health England, Middle East Respiratory Syndrome (MERS-CoV) Infection Prevention and Control Guidance, Public Health England, London, 2016, pp. 1–19.
[16] R. Mostofi, B. Wang, F. Haghighat, A. Bahloul, L. Jaime, Performance of mechanical filters and respirators for capturing nanoparticles-limitations and future direction, Ind. Health 48 (2010) 296–304.
[17] A. Rengasamy, Z. Zhuang, R. Berryann, Respiratory protection against bioaerosols: literature review and research needs, Am. J. Infect. Control 32 (2004) 345–354.
[18] H.P. Lee, D.Y. Wang, Objective assessment of increase in breathing resistance of N95 respirators on human subjects, Ann. Occup. Hyg. 55 (2011) 917–921.
[19] D.A. Japuntich, Respiratory particulate filtration, J. Int. Soc. Respir. Prot. 2 (1984) 137–169.
[20] A.T. Johnson, Respirator masks protect health but impact performance: a review, J. Biol. Eng. 10 (2016) 4.
[21] S.Y. Cho, et al., MERS-CoV outbreak following a single patient exposure in an emergency room in South Korea: an epidemiological outbreak study, Lancet 388

(2016) 994–1001.
[22] Air Pollution Control Technology Fact Sheet, EPA-452/F-03-029.
[23] A. Jaworek, A. Krupa, T. Czech, Modern electrostatic devices and methods for exhaust gas cleaning: a brief review, J. Electrostat. 65 (2007) 133–155.
[24] A. Zukeran, P.C. Looy, A.A. Berezin, J.S. Chang, T. Ito, Enhancement of electrostatic precipitator ultrafine particle collection efficiency by prechargers, J. Aerosol Sci. 28 (1997) S281–S282.
[25] M. Kocik, J. Dekowski, J. Mizeraczyk, Particle precipitation efficiency in an electrostatic precipitator, J. Electrostat. 63 (2005) 761–766.
[26] Z. Zhao, G. Zhang, New model of electrostatic precipitation efficiency accounting for turbulent mixing, J. Aerosol Sci. 23 (1992) 115–121.
[27] B. Navarette, L. Canadas, V. Cortes, L. Salvador, J. Galindo, Influence of plate spacing and ash resistivity on the efficiency of electrostatic precipitators, J. Electrostat. 39 (1997) 65–81.
[28] G. Mainelis, A. Adhikari, K. Willeke, S.A. Lee, T. Reponen, S.A. Grinshpun, Collection of airborne microorganisms by a new electrostatic precipitator, J. Aerosol Sci. 33 (2002) 1417–1432.
[29] B. Chua, A.S. Wexler, N.C. Tien, D.A. Niemeier, B.A. Holmén, Design, fabrication and testing of microfabricated corona ionizer, J. Microelectromech. Syst. 17 (2008) 115–123.
[30] B. Chua, A.S. Wexler, N.C. Tien, D.A. Niemeier, B.A. Holmén, Electrical mobility separation of airborne nanoparticles using integrated microfabricated corona ionizer and separator electrodes, J. Microelectromech. Syst. 18 (2009) 4–13.
[31] B. Chua, A.S. Wexler, N.C. Tien, D.A. Niemeier, B.A. Holmén, Collection of liquid phase particles by microfabricated electrostatic precipitator, J. Microelectromech. Syst. 22 (2013) 1010–1019.
[32] B. Chua, A.S. Wexler, N.C. Tien, D.A. Niemeier, B.A. Holmén, Micro-corona based particle steering air filter, Sens. Actuators A-Phys. 196 (2013) 8–15.
[33] E.-H. Lee, H.J. Lim, B. Chua, A. Son, Detection of airborne bacteria with disposable bio-precipitator and NanoGene assay, Biosens. Bioelectron. 83 (2016) 205–212.
[34] W. Li, S.T. Oyama, Mechanism of ozone decomposition on a manganese oxide catalyst: steady-state and transient kinetic studies, J. Am. Chem. Soc. 120 (1998) 9047–9052.
[35] K.R. Parker, Applied Electrostatic Precipitation, Blackie Academic & Professional, London, 1997.
[36] W.C. Hinds, Aerosol Technology: Properties, Behavior and Measurement of Airborne Particles, John Wiley & Sons, New York, 1999.
[37] R.C. Flagan, History of aerosol measurement, Aerosol Sci. Technol. 28 (1998) 301–380.
[38] A.S. Wexler, M.V. Johnson, P.A. Baron, K. Wileke (Eds.), Real-Time Single Particle Analysis. Aerosol Measurement, John Wiley & Sons, New York, 2001.
[39] W.C. Adams, Measurement of Breathing Rate and Volume in Routinely Performed Activities, National Technical Information Service, NTIS No. PB94109444, 1993 Contract No. A033-205.
[40] J.R. Holmes, How Much Air do We Breathe? Brief Reports to the Scientific and Technical Community, California Environmental Protection Agency, 1994 Research Note 94-11.
[41] I. Araron, J. Prussin, E.B. Garcia, L.C. Marr, Total concentrations of virus and bacteria in indoor and outdoor air, Environ. Sci. Technol. Lett. 2 (2015) 84–88.
[42] T. Fujino, S. Yamaguchi, T. Hattori, Formation of manganese dioxide coating with catalytic activity on thick boehmite film by hydrothermal method, Mater. Trans. 46 (2005) 3026–3029.
[43] S.K. Kalilasa, H.-F. Wu, Surface modified BaTiO3 nanoparticles as the matrix for phospholipids and as extracting probes for LLME of hydrophobic proteins in Escherichia coli by MALDI–MS, Talanta 114 (2013) 283–290.
[44] G. Kim, A. Son, Development and characterization of a magnetic bead-quantum dot nanoparticles based assay capable of Escherichia coli O157:H7 quantification, Anal. Chim. Acta 677 (2010) 90–96.

Miri Park received her B.S. (2016) and M.S. (2018) in environmental engineering from Ewha Womans University, Seoul, Republic of Korea. Her research interests are micro corona ionizers, catalytic reactions and air purification.

Ahjeong Son received her B.S. (1998) and M.S. (2000) in Environmental Engineering from Ewha Womans University and GIST in Republic of Korea, respectively. She received her Ph.D. (2005) in Civil and Environmental Engineering from University of Delaware. She was a postdoctoral researcher in the Department of Land, Air, and Water Resources at University of California, Davis in 2005–2008. She worked as an Assistant/Associate Professor in the Department of Civil Engineering at Auburn University in 2008–2015. She is currently an Associate Professor in the Department of Environmental Engineering at Ewha Womans University, Seoul, Republic of Korea. Her research interests include environmental biosensors, environmental microbiology, and biological process and dynamics.

Beelee Chua received B.Eng. and M.Eng. degrees in mechanical engineering from the National University of Singapore in 1999 and 2001 respectively, and Ph.D. degree in electrical engineering from University of California, Davis in 2005. He was a member of Berkeley Sensor and Actuator Center (BSAC) before joining a biomedical device startup company in the San Francisco Bay Area. He is currently an Associate Professor in the School of Electrical Engineering, Korea University, Korea. His research interest revolves around small reactive responsive systems. They currently include high voltage micro devices, micro corona ionizers and applications, on-patient diagnostics and therapeutics as well as environmental monitoring systems and devices.